Research article

Carbon Future

# Unveiling the Eley–Rideal mechanism: $H_2$ activation for nitrobenzene hydrogenation on nitrogen-doped carbon nanotubes

Hongquan Fu [1,2], Kuntao Huang[1], Jialong Zhang[3] ✉, Yonghai Cao[1], Hongjuan Wang[1], Hejun Gao[2], Yunwen Liao[2], Shuang Li[3], and Hao Yu [1] ✉

[1] School of Chemistry and Chemical Engineering, Guangdong Provincial Key Lab of Green Chemical Product Technology, South China University of Technology, Guangzhou 510640, China
[2] Chemical Synthesis and Pollution Control Key Laboratory of Sichuan Province, Institute of Applied Chemistry, College of Chemistry and Chemical Engineering, China West Normal University, Nanchong 637000, China
[3] School of Biology and Biological Engineering, South China University of Technology, Guangzhou 510006, China

Cite This: *Carbon Future* **2025**, *2*, 9200028

Read Online

**ABSTRACT:** Nitrogen-doped carbon nanotubes (NCNTs) emerge as an efficient metal-free catalyst for the hydrogenation of nitrobenzene to aniline, utilizing molecular hydrogen ($H_2$) as the reducing agent. However, the mechanism of $H_2$ activation on NCNTs is under debate so far. Here, we unveil the catalytic mechanism of NCNTs in this reaction through a comprehensive approach combining experimental and theoretical investigations. Our findings indicate that NCNTs are unable to directly dissociate $H_2$ molecules, suggesting that the hydrogenation reaction does not proceed via the conventional Horiuti–Polanyi mechanism. Instead, we propose an Eley–Rideal mechanism, where $H_2$ molecules are activated upon adsorption on the surface of NCNTs with adsorbed nitrobenzene molecules. Graphitic nitrogen ($N_G$) and pyridine nitrogen ($N_P$) are identified as the primary active sites. However, at higher nitrogen contents, the synergistic interaction between $N_P$ and $N_G$ is detrimental to catalytic activity, emphasizing that increased nitrogen content does not necessarily enhance performance. Further experiments demonstrate that, in addition to direct $H_2$ activation, the transfer hydrogenation in protic solvents significantly boosts the overall reaction rate. Our work provides deep insights into the mechanism of $H_2$ activation for the nitrobenzene hydrogenation catalyzed by NCNTs and offers theoretical guidance for the rational design of high-performance metal-free catalysts in catalytic hydrogenation reactions.

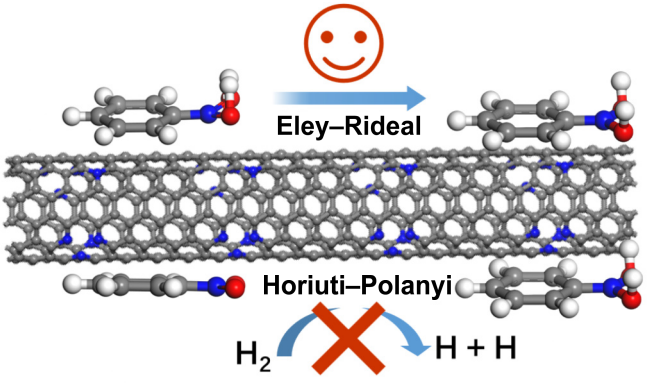


**KEYWORDS:** carbon catalysis, hydrogenation, graphitic nitrogen, pyridinic nitrogen, synergistic effect, DFT calculation

## 1 Introduction

The catalytic hydrogenation plays an important role in various fundamental chemical transformations, including in the food, agricultural, and pharmaceutical industries[1]. Most hydrogenation catalysts contain metal as active centers, suffering from the leaching, sintering, and limited sources. In contrast, metal-free carbon-based materials are eco-friendly, abundant, and readily available heterogeneous catalysts for organic hydrogenation reactions[2]. The construction of functional groups on the surface of carbon materials as non-metal catalysts for catalytic hydrogenation has attracted wide attentions[3]. Kong et al. found that nitrogen-doped graphenes catalyzed the reduction of nitrobenzene to aniline by sodium borohydride, and its catalytic reduction characteristics were significantly different from those of metal catalysts[4]. The strong reducing reagents such as hydrazine hydrate ($N_2H_4{\cdot}H_2O$) and sodium borohydride ($NaBH_4$) were generally required to promote the hydrogenation activity[5]. Chen et al.[6] found that phosphorus-doped carbon nanotubes, showing metal-like properties, can efficiently promote metal-free hydrogenation of nitrobenzene to aniline using $N_2H_4{\cdot}H_2O$ and molecular hydrogen ($H_2$) as reducing reagents. Obviously, direct and clean hydrogenation of nitroaromatics with $H_2$ is highly desirable from the viewpoint of green and sustainable chemistry. Xu et al.[7] reported the synergistic

**Received:** October 28, 2024; **Revised:** December 16, 2024
**Accepted:** December 17, 2024

✉Address correspondence to Jialong Zhang, 917909363@qq.com; Hao Yu, yuhao@scut.edu.cn

https://doi.org/10.26599/CF.2025.9200028

catalysis of mixed $C_{60}$ and $C_{60}^-$ fullerene in the reduction of aromatic nitro compounds to amines using $H_2$, without the addition of any metal salts. Very high conversion rate and selectivity of up to 100% were achieved. However, the carbonaceous materials appliable for $H_2$ activation in hydrogenation reactions are greatly limited so far, due to their weak adsorption capacity for $H_2$ and the challenge in dissociating $H_2$ on their surfaces.

It is crucial to explore the mechanism of activation of $H_2$ on metal-free carbon materials for the rational design of high-performance hydrogenation catalysts. In 2006, Stephan and co-workers found that sterically encumbered phosphorus and borane acids and bases (called "frustrated Lewis pairs (FLPs)") can promote heterolytic cleavage of $H_2$[8, 9]. Due to its strong polarization ability[10], FLPs heterolytically cleave molecular hydrogen, thereby activating it under mild conditions[11, 12]. Su and co-workers[13] confirmed that B–N Lewis pairs at the edges of carbon materials can split $H_2$ to form $H^+/H^-$ pairs, which subsequently serve as the active species for hydrogenation of unsaturated double bonds and nitro functional groups. The continuous expansion commenced by utilizing carbon materials doped with heteroatoms, such as N[14] and P[6], as catalysts for hydrogenation. Shan et al.[14] found that the activity of nitrogen-doped carbon nanotubes (NCNTs) in catalyzing the reduction of nitrophenol by $H_2$ in tert-amyl alcohol solvent is related to the graphitic nitrogen content and diameter (10–20 nm). Subsequently, they proposed that the pyrrolic and graphitic nitrogen on the surface of carbon materials are the active sites for catalyzing the hydrogenation of nitrophenol[15]. Liu and co-workers[16] identified that the active sites for catalyzing the hydrogenation reaction of nitrobenzene reduction by $H_2$ in ethanol solvent are pyrrolic nitrogen. Qi's group[17] reported metal-free nitrogen-assembly carbons (NACs) with closely-placed graphitic nitrogen as active sites, achieving dihydrogen dissociation and subsequent transformation of oxygenates. Despite the achievements employing carbon materials in catalytic hydrogenation, the controversy over the active sites of catalytic hydrogenation indicates the lack of understanding to the hydrogenation mechanism.

Direct evidences for the hydrogen activation on FLPs have been reported in Ref.[18]. The insufficiency in evidence regarding the activation of $H_2$ on carbon materials may stem from the following aspects: (1) The correlation between the content of active sites and activity appears to be weak, suggesting the overlooked synergistic effects[17]. (2) Most carbon-catalyzed hydrogenations of nitrobenzene have been conducted in protic solvents[16], leading to the uncertainty of the source of active hydrogen. (3) It has been reported that the adsorption capacity of $H_2$ molecules on the surface of nitrogen-doped carbon materials was even lower than that of pure carbon materials[19], and the interaction between the adsorbed species and carbon was weak[20]. Therefore, the mechanism by which carbon materials directly activate $H_2$ and dissociate it into H atoms remains unclear.

In this study, we seek to explore the catalytic hydrogenation of nitrobenzene occurring on the surface of nitrogen-doped carbons (NCs) across wide range of nitrogen contents. Our objective is to uncover the mechanism of $H_2$ activation on NCs via investigating the effect of solvent, the structure–activity relationship, and the kinetics of hydrogenation to determine whether the hydrogenation process follows the Horiuti–Polanyi (H–P) or Eley–Rideal (E–R) mechanism. By doing so, we aim to guide the rational design of catalysts and unravel the complex interplay between catalyst structure and activity. Ultimately, our goal is to establish a theoretical framework that will facilitate the advancement of non-metallic catalytic hydrogenation.

## 2 Results and discussion

As shown in **Table 1**, undoped carbon nanotubes (CNTs) and oxidized CNTs do not exhibit catalytic activity for the hydrogenation of nitrobenzene. However, NCNTs prepared by the pyridine deposition at 700 °C for 0.3 h exhibits excellent catalytic activity, with a nitrobenzene conversion of 66% and a reaction rate of 10.54 $mmol \cdot g^{-1} \cdot h^{-1}$. As the deposition time of pyridine on the carbon material increased from 0.3 to 4.0 h, the conversion of nitrobenzene gradually decreases from 66.0% to 2.1%, and the mass-normalized reaction rate ($r$) of nitrobenzene gradually decreases from 10.54 to 0.33 $mmol \cdot g^{-1} \cdot h^{-1}$. The similar trend was ascertained by normalizing the reaction rate to surface area to exclude the effect of declined surface area of NCNTs-$t$ with long deposition durations (see Table 1). This abnormal dependence of activity on N-doping implies that the catalytic hydrogenation of nitrobenzene on NCs in isopropanol is very sensitive to the nitrogen content.

To discriminate the active sites of NCNTs-$t$ catalyzing the hydrogenation of nitrobenzene, the influence of nitrogen content (ranging from 0.00% to 5.70%, determined by elemental analysis in Supplementary Table S1) on the catalytic activity was investigated by varying the pyridine deposition time. As shown in **Fig. 1a** and Supplementary Table S1, although the undoped CNTs exhibits no activity, the NCNTs-0.3 h shows the highest activity with quite low nitrogen content of 0.98% by X-ray photoelectron spectroscopy (XPS) analysis, indicating that the introduction of nitrogen indeed boosts the activity for the hydrogenation of nitrobenzene. However, as the nitrogen content increased with the increasing deposition time, the activity gradually decreased. When the gross nitrogen content increased, the content of pyridinic nitrogen ($N_P$) and graphitic nitrogen ($N_G$) increased from 0.27% to 2.04% and from 0.26% to 2.84%, respectively. Figs. 1b and 1c show that the specific activity also decreases with the increase of $N_P$ and $N_G$ contents, indicating that the increase of $N_P$ and $N_G$ contents suppresses the catalytic activity of nitrobenzene hydrogenation. Furthermore, the scattered points observed in Fig. 1d, which represent the relationship between the content of pyrrolic nitrogen ($N_{Pyr}$) and the reaction rate, suggest a relatively weak correlation between the two variables. The aforementioned results indicate that the active sites could be formed by multiple assemblies, specifically exhibiting a synergistic effect among nitrogen species, possibly including $N_P$ and $N_G$[21].

As previously reported[22], a decrease in the distance between nitrogen sites at elevated concentrations may give rise to an unfavorable synergistic effect that hinders reaction activity in the oxidation of styrene. The abnormal dependence of the activity in the hydrogenation of nitrobenzene indicates a similar interplay between nitrogen species. To verify this, the catalyst NCNTs-4.0 h was annealed at 1100 °C to reduce the content of $N_P$, while the $N_G$ content remained almost unchanged (see Supplementary Table S1). Under the same conditions, the nitrobenzene hydrogenation reaction was catalyzed by NCNTs-4.0 h-H (referring to NCNTs-4.0 h annealed at 1100 °C), resulting in a 20.9% increase in the conversion rate of nitrobenzene compared to NCNTs-4.0 h. This confirms that reducing nitrogen content in cases of high nitrogen levels can enhance reaction activity. The unique behavior of NCNTs enables a remarkable enhancement in hydrogenation activity even with a minimal doping level of nitrogen, highlighting the crucial role of modifying the doping process. It is worth mentioning that both $N_G$ and $N_P$ contribute positively to the activity at low total N contents[22], suggesting their potential to serve

**Table 1 Catalytic activity of NCs for nitrobenzene hydrogenation**

| Catalyst | $S_{BET}$ ($m^2 \cdot g^{-1}$) | PV ($cm^3 \cdot g^{-1}$) | Conv. (%) | $S_{PhNH_2}$ (%)[a] | $r$ ($mmol \cdot g^{-1} \cdot h^{-1}$)[b] | $r_s$ ($mmol \cdot m^{-2} \cdot h^{-1}$)[c] |
|---|---|---|---|---|---|---|
| — | — | — | 0.0 | 0.0 | — | — |
| Oxidized CNTs | 201 | — | 0.0 | 0.0 | 0.00 | 0.00 |
| CNTs | 178 | 0.84 | 0.0 | 0.0 | 0.00 | 0.00 |
| NCNTs-0.3 h-500 | 154 | — | 0.0 | 0.0 | 0.00 | 0.00 |
| NCNTs-0.3 h-600 | 156 | — | 0.0 | 0.0 | 0.00 | 0.00 |
| NCNTs-0.3 h | 161 | 0.36 | 66.0 | 100.0 | 10.54 | 0.065 |
| NCNTs-0.5 h | 164 | 0.72 | 32.4 | 100.0 | 5.04 | 0.031 |
| NCNTs-1.0 h | 133 | 0.57 | 12.2 | 100.0 | 1.88 | 0.014 |
| NCNTs-1.5 h | 117 | 0.60 | 9.2 | 100.0 | 1.41 | 0.012 |
| NCNTs-2.0 h | 122 | 0.20 | 6.7 | 100.0 | 1.02 | 0.008 |
| NCNTs-4.0 h | 121 | 0.24 | 2.1 | 100.0 | 0.33 | 0.003 |
| NCNTs-4.0 h-H | 104 | — | 23.0 | 100.0 | 3.57 | 0.034 |

Reaction conditions: 50 mg of catalyst, 18 mL of isopropanol as solvent, 2 MPa $H_2$, 140 °C, and 5 h.
[a]Selectivity to aniline ($PhNH_2$).
[b]Reaction rate of $PhNO_2$ consumption normalized by catalyst mass: $r = \frac{n_{0,PhNO_2} \times X}{m_{cat.} \times t} \times 100\%$, where $n_{0,PhNO_2}$ is the initial amount of $PhNO_2$, $X$ is the conversion of $PhNO_2$, $t$ is the reaction time of 5 h, and $m_{cat.}$ is the mass of catalyst.
[c]Reaction rate of $PhNO_2$ consumption normalized by specific surface area of the catalyst: $r_s = \frac{r}{S_{BET}}$, where $S_{BET}$ is the specific surface area of the catalyst.

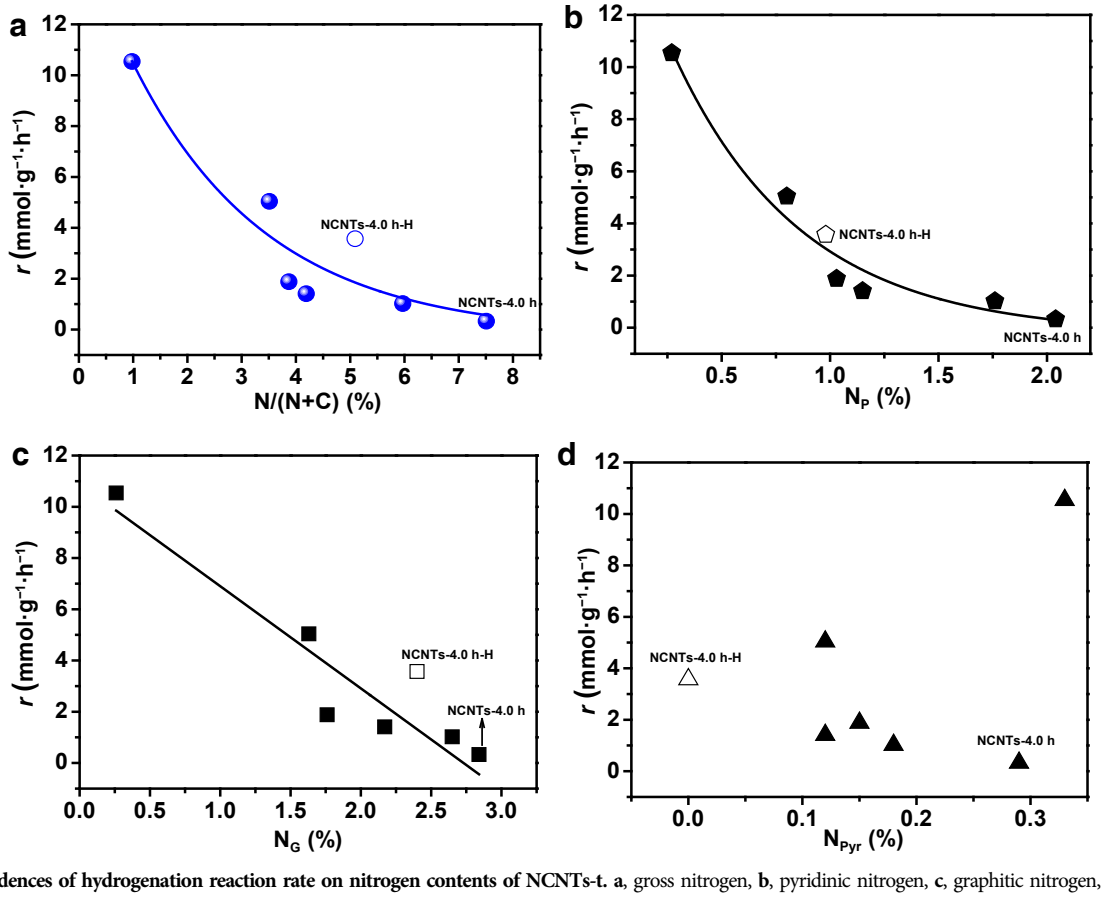


**Fig. 1. Dependences of hydrogenation reaction rate on nitrogen contents of NCNTs-t. a**, gross nitrogen, **b**, pyridinic nitrogen, **c**, graphitic nitrogen, **d**, pyrrolidine nitrogen. The nitrogen contents were measured by XPS.

as active sites for the process of catalytic hydrogenation when they are isolated and free from interaction. In the subsequent sections, we utilize density functional theory (DFT) calculations to confirm the previously mentioned scenario.

Compared to various catalysts (including metal oxides, phosphorus-doped carbon catalysts, and nitrogen-doped carbon catalysts[23]) listed in Supplementary Table S2, NCNTs-0.3 h exhibits excellent catalytic activity and outstanding selectivity for aniline

(~ 100%). The NCNTs exhibited remarkable stability, maintaining consistent performance over five repeated cycles in isopropanol solvent, as illustrated in Supplementary Fig. S1. Those findings indicate that NCNTs represent a promising metal-free catalyst for the nitrobenzene hydrogenation.

In catalytic hydrogenation reactions, isopropanol as a protic solvent can provide protons, which facilitates the transfer hydrogenation, thus interfering the identification of the pathway of active hydrogen species[24]. As shown in **Table 2**, using NCNTs-0.3 h as the catalyst, a conversion of approximately 0.6% can still be measured for the hydrogenation of nitrobenzene in isopropanol solvent even under $N_2$ atmosphere, with a specific activity of 0.10 mmol·g$^{-1}$·h$^{-1}$. However, under the same conditions, the blank reaction without catalyst exhibits no catalytic activity. This result indicates that the nitrobenzene transfer hydrogenation catalyzed by NCs in isopropanol solvent cannot be neglected. The transfer hydrogenation reaction in isopropanol solvent leads to the formation of aprotic acetone, in which a significantly improved specific activity of 1.27 mmol·g$^{-1}$·h$^{-1}$ was observed. It suggests that NCs can activate and utilize molecular $H_2$ without the aid of protic solvents. To further exclude the influence of transfer hydrogenation, the aprotic solvents such as acetonitrile, n-heptane, and carbon tetrachloride were selected to carry out the hydrogenation of nitrobenzene. Using NCNTs-0.3 h as the catalyst and under the same conditions, the specific hydrogenation activities ($r$) of nitrobenzene in acetonitrile, n-heptane, and carbon tetrachloride were determined as 1.45, 1.51, and 1.15 mmol·g$^{-1}$·h$^{-1}$, respectively. In addition, the specific activity under solvent-free conditions was 0.90 mmol·g$^{-1}$·h$^{-1}$. When 0.025 g of 2,6-di-tert-butyl-4-methylphenol (BHT) with protonation ability was added into aprotic acetonitrile, the consumption rate of nitrobenzene was significantly improved from 1.45 to 3.91 mmol·g$^{-1}$·h$^{-1}$, confirming the interplay of transfer hydrogenation in protic solvents with the direct activation of $H_2$. In protic isopropanol solvent, the hydrogenation activity reached 10.45 mmol·g$^{-1}$·h$^{-1}$, more than 7 folds of that in aprotic acetonitrile solvent. Hence, protic solvents should not be applied for exploring the activation of molecular dihydrogen, despite the enhanced apparent activity[25], because such proton addition processes may compete with the direct catalytic hydrogenation process.

It is highly desired to ascertain whether and how active hydrogen species are produced from molecular dihydrogen upon exposure to NCs, as well as the mechanism behind this generation. To this end, the activation of $H_2$ was investigated by comparing NCNTs with Pd/C, a well-established hydrogenation catalyst that can dissociate $H_2$ to generate active atomic hydrogen (**Fig. 2**). Fig. 2a shows the quasi *in-situ* electron paramagnetic resonance (EPR) results of commercial Pd/C catalyst in aprotic acetonitrile or protic isopropanol solvent. In aprotic acetonitrile without nitrobenzene, EPR spectrum obtained from the solution after its interaction with the catalyst exhibits hyperfine interactions (hfi) characterized with a single nitrogen nucleus and two equivalent hydrogen nuclei. By comparing this spectrum with well-documented spectra and hfi values for the monohydrogen atom adduct of N-tert-butyl-α-phenylnitrone (PBN), it can be confidently attributed to the hydrogen atom spin adduct[26]. In protic isopropanol without nitrobenzene, the sole distinction lies in the diminished resolution, causing the nine lines, manifested as a triplet of triplets, to merge, resulting in a seven-line spectrum exhibiting apparent intensities of 1:2:2:2:2:2:1. The surface hydrogen ad-atoms must have considerable radical features, otherwise spin trapping would not be possible[27, 28]. In the presence of nitrobenzene, aprotic acetonitrile and protic isopropanol solvents both show merely the EPR characteristic for the addition of hydrogen atom to nitroso group, which results in the formation of $C_6H_5N$·OH nitroxyl radical[29]. The dissociation and activation of $H_2$ occur in both isopropanol and acetonitrile solvents, demonstrating the generation of hydrogen radicals by Pd/CNT catalyst. Furthermore, the radicals are active in the nitrobenzene hydrogenation, evidenced by the suppressed EPR signal in the presence of nitrobenzene and the obviously weaker signal in isopropanol due to the faster reaction rate. However, the EPR testing revealed no significant signals using NCNTs as catalyst even at elevated temperature and prolongated duration, either in isopropanol or acetonitrile. It indicates that $H_2$ splitting does not directly occur on NCNTs to produce hydrogen radicals that can be trapped by PBN under reaction conditions, regardless of whether

**Table 2 Effect of solvent on the nitrobenzene hydrogenation catalyzed by NCNTs**

| Catalyst | Gas | Solvent | $c_{PhNO_2}$ (mmol·mL$^{-1}$) | Con. (%) | $S_{PhNH_2}$ (%) | $r$ (mmol·g$^{-1}$·h$^{-1}$)[a] | $r_s$ (mmol·cm$^{-2}$·h$^{-1}$)[b] |
|---|---|---|---|---|---|---|---|
| NCNTs-0.3 h | $H_2$ | Isopropanol | 0.2216 | 66.0 | 100.0 | 10.45 | 0.065 |
| — | $N_2$ | Isopropanol | 0.2017 | 0.0 | — | 0.00 | 0.000 |
| NCNTs-0.3 h | $N_2$ | Isopropanol | 0.2112 | 0.6 | 100.0 | 0.10 | 0.001 |
| NCNTs-0.3 h | $H_2$ | $CH_3CN$ | 0.2185 | 9.2 | 100.0 | 1.45 | 0.009 |
| NCNTs-0.3 h | $N_2$ | $CH_3CN$ | 0.2238 | 0.0 | — | 0.00 | 0.000 |
| NCNTs-0.3 h | $H_2$ | n-heptane | 0.2151 | 9.8 | 100.0 | 1.51 | 0.009 |
| NCNTs-0.3 h | $H_2$ | Acetone | 0.2188 | 8.1 | 60.0 | 1.27 | 0.008 |
| NCNTs-0.3 h | $H_2$ | $PhNO_2$[c] | — | 0.3 | 100.0 | 0.90 | 0.006 |
| NCNTs-0.3 h | $H_2$ | $CCl_4$ | 0.2228 | 7.4 | 100.0 | 1.15 | 0.007 |
| NCNTs-0.3 h + BHT | $H_2$ | $CH_3CN$ | 0.2275 | 23.8 | 100.0 | 3.91 | 0.024 |

Reaction conditions: 50 mg of catalyst, 18 mL of solvent, 140 °C, 2 MPa, and 5 h.

[a]Reaction rate of $PhNO_2$ consumption normalized by catalyst mass: $r = \frac{n_{0,PhNO_2} \times X}{m_{cat.} \times t} \times 100\%$, where $n_{0,PhNO_2}$ is the initial amount of $PhNO_2$, $X$ is the conversion of $PhNO_2$, $t$ is the reaction time, and $m_{cat.}$ is the mass of catalyst.

[b]Reaction rate of $PhNO_2$ consumption normalized by specific surface area of the catalyst: $r_s = \frac{r}{S_{BET}}$, where $S_{BET}$ is the specific surface area of the catalyst.

[c]Solvent-free, 9.2142 g of $PhNO_2$.

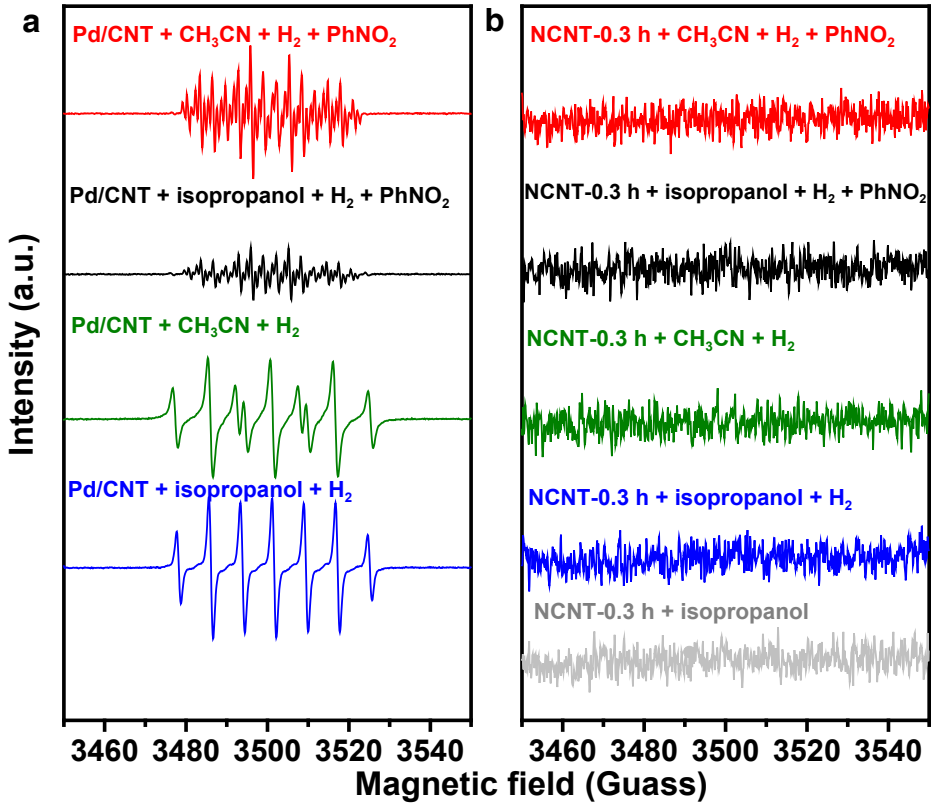


**Fig. 2. EPR spectra using N-benzylidene-tert-butylamine N-oxide (PBN) as the spin trap. a**, 50 mg of Pd/CNT, 18 mL of solvent, room temperature, 10 min, and 2 MPa $H_2$. **b**, 50 mg of NCNT-0.3 h, 18 mL of solvent, 140 °C, 0.5 h, and 2 MPa $H_2$.

the solvent is protic or aprotic. It suggests a very different hydrogenation mechanism of nitrobenzene on NCNTs from that on traditional metallic catalysts, e.g., Pd/C. The slower catalytic hydrogenation rate of NCNTs is attributed to the insufficiency of hydrogen radicals. Furthermore, the EPR results indicate that the entire process of nitrobenzene hydrogenation on NCNTs proceeds without the involvement of free radicals, suggesting that hydrogen molecules likely interact directly with nitrobenzene molecules to form –O–H bonds. Nonetheless, it remains possible that H–H bonds undergo heterocleavage on the surface of NCNTs even without detectable hydrogen radicals. It's worth noting that the adsorption capacity of nitrobenzene on NCNTs may significantly surpass that of hydrogen molecules due to the π–π interaction between the benzene ring and carbon materials[22]. This observation will be further elucidated through DFT calculations.

The absence of direct evidence regarding the activation of molecular hydrogen on NCNTs has driven our exploration into the kinetics of nitrobenzene hydrogenation. This investigation could potentially facilitate the discrimination between the direct activation of hydrogen molecules by NCNTs and the indirect activation mediated by nitrobenzene molecules adsorbed onto the surface of NCNTs. The influence of mass transfer was excluded by a stirring speed at 1100 r·min$^{-1}$ (Supplementary Fig. S2) to guarantee that the reaction conditions were within the kinetic region. **Fig. 3** displays the kinetic traits of catalytic hydrogenation of nitrobenzene in both protonic and non-protonic solvents on NCNTs-1.0 h for obtaining data with low conversions. As revealed by the ln($r$) versus ln($c_{PhNO_2}$) plot (Fig. 3a), the reaction rate ($r$) of nitrobenzene remains unaffected by variation in nitrobenzene concentration, suggesting that the hydrogenation catalyzed by NCNTs follows zero-order kinetics with respect to nitrobenzene. This implies that the reaction rate is predominantly affected by the availability of active sites on the catalyst. Apparently, nitrobenzene exhibits significant adsorption on NCNTs, while its surface coverage remains unaffected by its concentration in the liquid phase. This behavior stands in stark contrast to hydrogenation reactions catalyzed by metal catalysts, which typically follow first-order kinetics, as well-documented in Refs.[30, 31]. As shown in Fig. 3b, the ln($r$) versus ln($p_{H_2}$) plot reveals a linear correlation. The slopes of this linear relationship are 0.86 and 1.28 in isopropanol and acetonitrile, respectively, suggesting that the hydrogenation of nitrobenzene on NCNTs roughly follows first-order kinetics with respect to $H_2$. Similar kinetics behavior has been reported previously over P-doped and N-doped carbon materials[6, 17]. Chen et al.[6] proposed a FLP mechanism for the hydrogenation of nitrobenzene on P-doped CNTs, wherein the rate-determining step involves the heterolytic cleavage of $H_2$ on FLPs to generate active hydrogen. However, their kinetics study was conducted in protic methanol, excluding potential solvent effects. Furthermore, it is also unclear whether $H^+$ and $H^-$ from the heterolytic cleavage migrate or undergo H exchange with the solvent, thereby violating first-order reaction kinetics. Similarly, the solvent effect of propanol on the kinetics was not considered either in the case of metal-free nitrogen-assembly carbons[17]. Nevertheless, the second-order polynomial relationship between graphitic nitrogen content and activity[17] suggests very different activation mechanism from ours (Fig. 1c).

The reaction network for catalytic reduction of aromatic nitro compounds outlines two separate routes[32], as illustrated in Supplementary Fig. S3, namely the direct route and the condensation route. In the direct route, the aromatic nitro

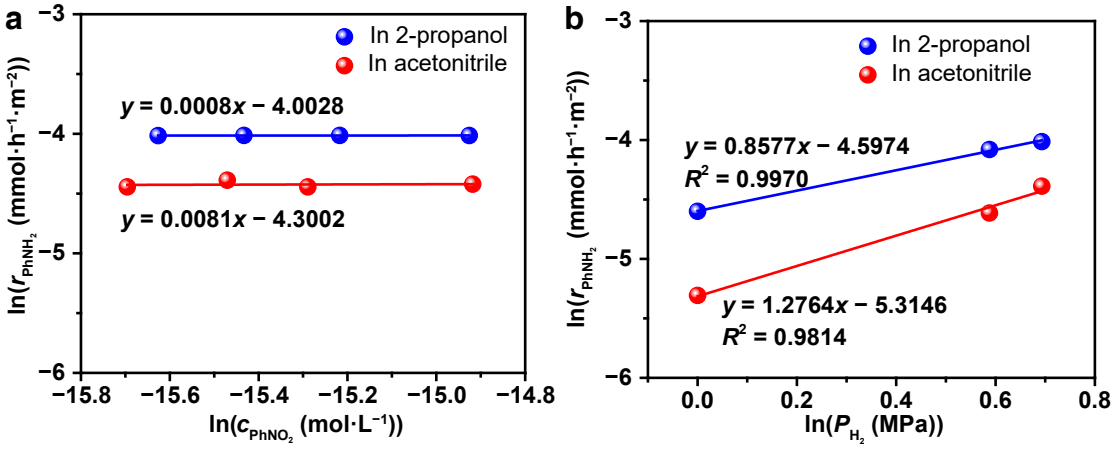


**Fig. 3. Kinetics study on the hydrogenation reaction. a**, **b**, Plots of reaction rate of aniline ($PhNH_2$) formation normalized by catalyst surface area ($r$) versus the concentration of nitrobenzene ($PhNO_2$) (a) and the partial pressure of $H_2$ (b). Reaction conditions: 50 mg of NCNTs-1.0 h, 140 °C, 2 h, and 18 mL of 2-propanol/acetonitrile.

compound ([$PhNO_2$]) progressively reduces to form the nitroso compound ([NSB]), subsequently converting to hydroxylamine ([PHA]), and ultimately yielding aniline ([$PhNH_2$]). Alternatively, the condensation route involves the union of a [NSB] and a [PHA] molecule, leading to the formation of the azoxy compound ([AOB]). This then undergoes consecutive reductions to produce azo ([AB]), hydrazo ([HAB]), and finally, aniline. According to the abovementioned kinetics results, the strong adsorption of $PhNO_2$ leads to Eq. (1) in quasi equilibrium. On this basis, the adsorption and activation of $H_2$ can be considered with three hypotheses to establish the kinetics: (i) As an analogous of metal catalysts, it is assumed that the hydrogen dissociatively adsorbed on NCNTs to form atomic hydrogens, and the first hydrogenation with one hydrogen is rate-determining, namely the H–P mechanism. (ii) The dissociative adsorption of $H_2$ is rate-determining in the case of weak adsorption on NCNTs. (iii) If $H_2$ cannot be directly adsorbed and activated on NCNTs, the hydrogenation may follows the Eley–Rideal mechanism, which allows for the direct reaction of molecular hydrogen with adsorbed $PhNO_2$. The mechanisms are summarized as follows

(i) Horiuti–Polanyi mechanism

$$PhNO_2 + \sigma \rightleftharpoons PhNO_2\sigma \quad (1)$$

$$H_2 + 2\sigma \rightleftharpoons 2H\sigma \quad (2)$$

$$PhNO_2\sigma + H\sigma \rightarrow PhNO_2H\sigma \quad \text{RDS} \quad (3)$$

(ii) Horiuti–Polanyi mechanism with weak adsorption of $H_2$

$$PhNO_2 + \sigma \rightleftharpoons PhNO_2\sigma \quad (4)$$

$$H_2 + 2\sigma \rightarrow 2H\sigma \quad \text{RDS} \quad (5)$$

$$PhNO_2\sigma + H\sigma \rightarrow PhNO_2H\sigma \quad (6)$$

(iii) Eley–Rideal mechanism

$$PhNO_2 + \sigma \rightleftharpoons PhNO_2\sigma \quad (7)$$

$$PhNO_2\sigma + H_2 \rightarrow NSB\sigma + H_2O \quad \text{RDS} \quad (8)$$

The mechanism (i) leads to an expression of reaction rate as follows

$$r_1 = \frac{k[PhNO_2]\,K_{NB}\sqrt{K_{H_2}P_{H_2}}}{1 + K_{PhNO_2}[PhNO_2] + \sqrt{K_{H_2}P_{H_2}}} \quad (9)$$

where $K$ and $k$ represent the adsorption equilibrium constant and reaction rate constant of Eq. (3), respectively, $P$ is the partial pressure, and RSD is the rate-determining step. Considering the strong adsorption of $PhNO_2$ revealed by our experiments, the reaction rate expression can be simplified as $r_1 = k_1^{obs}\sqrt{P_{H_2}}$. The reaction order of 0.5 with respect to $H_2$ is inconsistent with the experimental result, suggesting that the H–P mechanism similar to metallic catalysts cannot explain the hydrogenation on NCNTs.

If the adsorption of $H_2$ is difficult in the H–P mechanism (mechanism (ii)), the reaction rate can be expressed as

$$r_2 = \frac{k_a P_{H_2}}{(1 + K_{PhNO_2}[PhNO_2])^2} \quad (10)$$

With the assumption of strong adsorption of $PhNO_2$, it can be simplified as $r_2 = k_2^{obs}P_{H_2}$, being consistent with the kinetics experiments. However, it violates the observed zero-order kinetics with respect to $PhNO_2$. Moreover, if the hydrogenation reaction of nitrobenzene proceeds via the Eley–Rideal mechanism (mechanism (iii)), the rate equation is as follows

$$r_3 = \frac{k[PhNO_2]\,K_{PhNO_2}P_{H_2}}{1 + K_{PhNO_2}[PhNO_2]} = k_3^{obs}P_{H_2} \quad (11)$$

In both mechanisms (ii) and (iii), the dependence of reaction rate on the hydrogen pressure agrees with the experimental observation, namely the first-order kinetics with respect to $H_2$. Another interpretation on the first-order kinetics by Chen et al.[6] assumes that the hetero-cleavage of $H_2$ on FLPs and the consequent adsorption of nitrobenzene nearby. However, there is no evidence for the formation of FLPs on N-doped carbon[13]. Besides that, mechanism requires the formation of surface complex between nitrobenzene and adjacent $H^+$ and $H^-$ from the hetero-cleavage, which may be limited by the supply of nitrobenzene. Next, we will discriminate the mechanisms (ii) and (iii) via DFT calculations.

One of the major differences between mechanisms (ii) and (iii) is whether $H_2$ is dissociatively activated into H atoms. The dissociation pathway of $H_2$ on carbon materials in acetonitrile is computed and compared in **Fig. 4**. Four geometric structures of the graphene-based catalysts were employed to conduct the DFT

calculation. The geometries include pristine graphene without dopants (G), graphene with a graphitic nitrogen dopant ($G_G$), graphene with a vacancy surrounding by three pyridinic nitrogen ($G_P$), and a combination of $G_G$ and $G_P$, denoted as $G_{PG}$. The design of the geometries for revealing the catalysis of typical nitrogen species and their synergistic effect has been depicted in our previous work[22]. The dissociation process commences from the ground states $^1G + H_2$, $^2G_G + H_2$, $^1G_P + H_2$, and $^2G_{PG} + H_2$, eventually leading to the formation of two adsorbed H atoms. The calculation of the formation energy suggests that, in terms of thermodynamics,

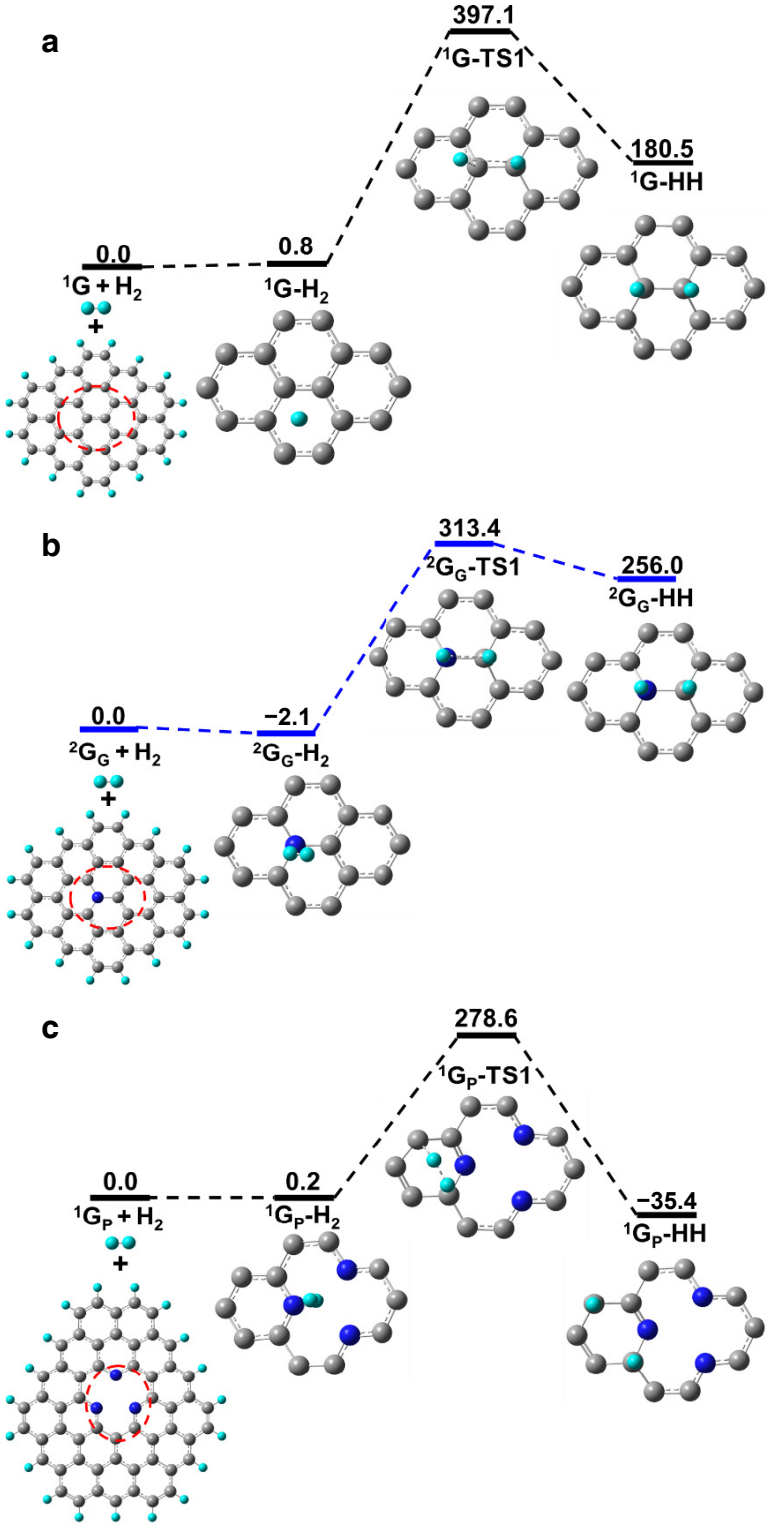


**Fig. 4. DFT calculation for the direct activation of $H_2$. a–d**, The optimized geometric structures and the schematic energy diagrams for the activation of $H_2$ on G (a), $G_G$ (b), $G_P$ (c), and $G_{PG}$ (d). Energies (kJ·mol$^{-1}$) relative to the ground state reactants $^1G + H_2$, $^2G_G + H_2$, $^1G_P + H_2$, and $^2G_{PG} + H_2$ at the B3LYP-D3(BJ)/6-311G(d,p)(SMD, $CH_3CN$) level are depicted. Black and blue lines represent the singlet and doublet states, respectively. Legend: gray: carbon, blue: nitrogen, and cyan: hydrogen.

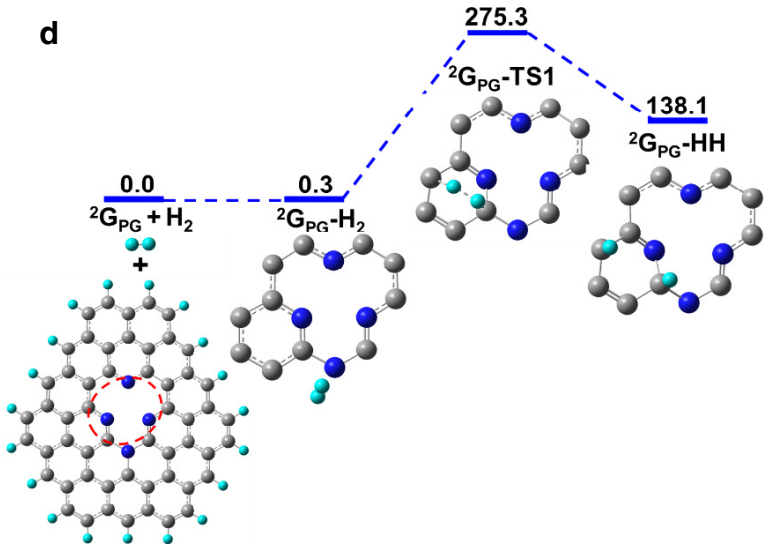


**Fig. 4.** Continued.

$G_{PG}$ is the most favorable for $H_2$ dissociation compared to G, $G_G$, and $G_P$, while the dissociation over $G_G$ is the most energy consuming. We explored the potential energy surface to delve deeply into the kinetic aspects of $H_2$ activation. $H_2$ molecules adsorb onto the surfaces of G, $G_G$, $G_P$, and $G_{PG}$, forming molecular complexes denoted as $^1$G-$H_2$, $^2G_G$-$H_2$, $^1G_P$-$H_2$, and $^2G_{PG}$-$H_2$, respectively. The adsorption energies for these complexes are 0.8, −2.1, 0.2, and 0.3 kJ·mol$^{-1}$, respectively, indicating that $G_G$ demonstrates superior ease in adsorbing and stabilizing $H_2$, forming more stable adsorbate. During the dissociation, the $H_2$ molecule transits through four-membered ring states, namely $^1$G-TS1, $^2G_G$-TS1, $^1G_P$-TS1, and $^2G_{PG}$-TS1. The highest energy barriers (HEB) of this transition are 396.3, 315.5, 278.4, and 275.0 kJ·mol$^{-1}$, respectively (as listed in Table 3). These high energy barriers render $H_2$ dissociation on NCNTs difficult. The energy height of the highest point (EHHP) on the reaction potential surface is a key indicator for the direct activation of $H_2$ molecules into H atoms. The $EHHP_{H_2}$ values for $H_2$ activation on G, $G_G$, $G_P$, and $G_{PG}$ surfaces are 397.1, 313.4, 278.6, and 275.3 kJ·mol$^{-1}$, respectively (Table 3). These high values suggest that the direct dissociation of $H_2$ on NCNTs via the H–P mechanism, i.e., mechanism (ii), is kinetically impractical.

The feasibility of E–R mechanism (mechanism (iii)) was theoretically assessed by DFT calculations in the presence of nitrobenzene molecule in acetonitrile. The reaction is initiated from the ground states, denoted as $^1$G + $H_2$ + $PhNO_2$, $^2G_G$ + $H_2$ + $PhNO_2$, $^1G_P$ + $H_2$ + $PhNO_2$, and $^2G_{PG}$ + $H_2$ + $PhNO_2$, as shown in **Fig. 5**. In terms of thermodynamics, these reactions result in the direct dissociation of $H_2$ forming adsorbed dihydroxyaniline on G, $G_G$, $G_P$, and $G_{PG}$, releasing exothermic energies of −64.1, −70.0, −64.4, and −61.8 kJ·mol$^{-1}$, respectively. This suggests that the hydrogenation of nitrobenzene is thermodynamically favorable, similar to the double H-induced dissociation mechanism to form $PhN(OH)_2$[33]. The kinetics analysis revealed that the initial hydrogenation of the first molecule is the critical step. Henceforth, our discussion will be confined to its activation mechanism, omitting further exploration of subsequent hydrogenation processes. To delve into the kinetic characteristics of the hydrogenation reaction, we explore the lowest potential energy surfaces. In the presence of nitrobenzene, the adsorption energies are determined as −51.6, −55.5, −56.1, and −53.6 kJ·mol$^{-1}$ on G, $G_G$, $G_P$, and $G_{PG}$, respectively, forming molecular complexes denoted as $^1$G-$PhNO_2$ + $H_2$, $^2G_G$-$PhNO_2$ + $H_2$, $^1G_P$-$PhNO_2$ + $H_2$, and $^2G_{PG}$-$PhNO_2$ + $H_2$, respectively. It indicates that nitrobenzene can stably adsorb on the surfaces of NCNTs forming stable intermediates. Compared to $H_2$, the adsorption of nitrobenzene is significantly more competitive, which agrees well with the experimental result of zero-order reaction with respect to nitrobenzene.

Subsequently, $H_2$ adsorbs onto the adsorbed nitrobenzene molecule to form co-adsorbed complexes denoted as $^1$G-$PhNO_2$-$H_2$, $^2G_G$-$PhNO_2$-$H_2$, $^1G_P$-$PhNO_2$-$H_2$, and $^2G_{PG}$-$PhNO_2$-$H_2$ with energies of −52.6, −55.7, −56.7, and −55.1 kJ·mol$^{-1}$, respectively, suggesting that $H_2$ acts to form stable co-adsorbates with nitrobenzene on the surfaces of G, $G_G$, $G_P$, and $G_{PG}$, enabling the E–R mechanism. As illustrated in Supplementary Fig. S4, $H_2$ adsorbed on nitrobenzene in the intermediates is prone to polarization for chemical adsorption, with charges of −0.004e, −0.005e, −0.004e, and −0.004e for $^1$G-$PhNO_2$-$H_2$, $^2G_G$-$PhNO_2$-$H_2$, $^1G_P$-$PhNO_2$-$H_2$, and $^2G_{PG}$-$PhNO_2$-$H_2$, respectively. It indicates that nitrobenzene adsorbed on graphite nitride facilitates polarizing $H_2$, and then the dissociation of $H_2$ from the surface-bound nitrobenzene molecules through tetra-ringed transition states is denoted as $^1$G-TS2, $^2G_G$-TS2, $^1G_P$-TS2, and $^2G_{PG}$-TS2. This dissociation forms intermediates in which two H atoms bind to the two oxygen atoms on nitrobenzene to form dihydroxyaniline with energy barriers of 216.3, 206.1, 213.1, and 212.9 kJ·mol$^{-1}$, respectively. These results validate the E–R mechanism of NC-catalyzed nitrobenzene hydrogenation. Significantly, the further dehydration of dihydroxyaniline results in the formation of aniline. The $EHHP_{N=O}$ on the reaction potential energy surface serves as a characteristic physical quantity for the hydrogenation through the E–R mechanism. The $EHHP_{N=O}$ values on G, $G_G$, $G_P$, and $G_{PG}$ are 163.7, 150.4, 156.4, and 157.8 kJ·mol$^{-1}$, respectively (Table 3). Notably, the $EHHP_{N=O}$ values for all nitrogen-doped graphene layers are lower than that of pristine graphene ($G_G$ < $G_P$ < $G_{PG}$ < G). It should be noted that $G_G$ exhibits the lowest $EHHP_{N=O}$ and $H_2$ dissociation barrier compared to $G_P$ and $G_{PG}$. It agrees with the fact that the hydrogenation activity reduces as the nitrogen doping content increases. The increasing population of vacant pyridinic nitrogen defects and adjacent graphitic and pyridinic nitrogen may decline the hydrogenation activity with the

increasing nitrogen content. This finding aligns with the reactivity of graphene nitrogen atoms in $H_2$ molecule dissociation, corroborating the results reported by Hu et al[34].

Above theoretical analysis suggests that the Eley–Rideal mechanism is more appliable for the hydrogenation of nitrobenzene catalyzed by NCNTs. At the meantime, our theoretical and experimental results show that NCs are unlikely to directly catalyze the dissociative activation of molecular hydrogen. It can be further supported by measuring the activation energy of nitrobenzene hydrogenation catalyzed by NCNTs. As shown in Supplementary Fig. S5, the Arrhenius plots indicate that the apparent activation energy in acetonitrile is 179.1 kJ·mol$^{-1}$. It is quite close to the result from DFT calculation of the E–R mechanism, but much lower than that in the H–P mechanism,

**Table 3 The EHHP and HEB (kJ·mol$^{-1}$) for the activation of $H_2$ and nitrobenzene hydrogenation reaction on G, $G_G$, $G_P$, and $G_{PG}$**

| Catalyst | $HEB_{H_2}$ | $HEB_{N=O}$ | $EHHP_{H_2}$ | $EHHP_{N=O}$ |
|---|---|---|---|---|
| G | 386.3 | 216.3 | 397.1 | 163.7 |
| $G_G$ | 315.5 | 206.1 | 313.4 | 150.4 |
| $G_P$ | 278.4 | 213.1 | 278.6 | 156.4 |
| $G_{PG}$ | 275.0 | 212.9 | 275.3 | 157.8 |

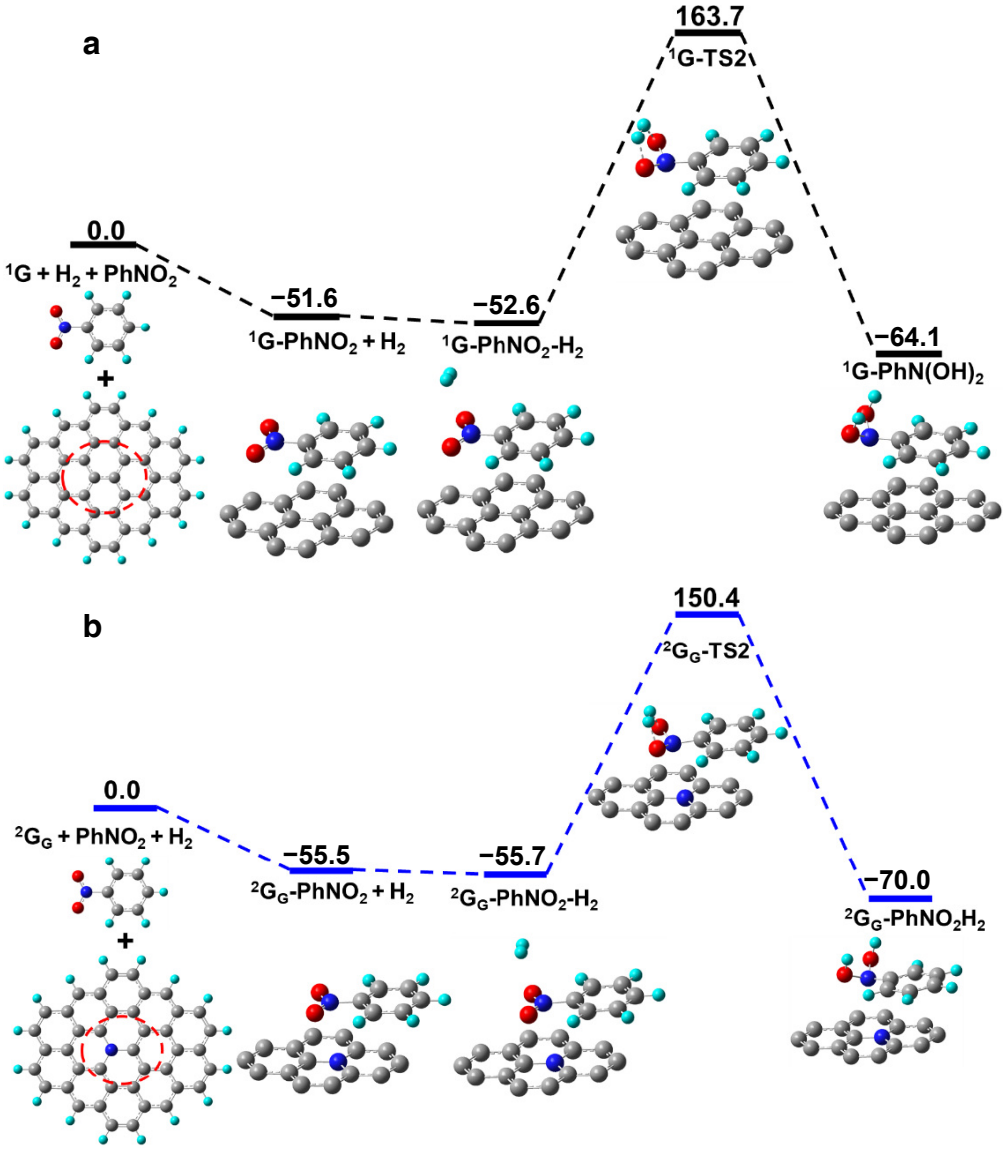


**Fig. 5. DFT calculation for the activation of $H_2$ via ER mechanism. a–d**, The optimized geometric structures and the schematic energy diagrams for the activation of $H_2$ on G (a), $G_G$ (b), $G_P$ (c), and $G_{PG}$ (d). Energies (kJ·mol$^{-1}$) relative to the ground state reactants $^1G$ + $PhNO_2$ + $H_2$, $^2G_G$ + $PhNO_2$ + $H_2$, $^1G_P$ + $PhNO_2$ + $H_2$, and $^2G_{PG}$ + $PhNO_2$ + $H_2$ at the B3LYP-D3(BJ)/6-311G(d,p)(SMD, $CH_3CN$) level are depicted. Black and blue lines represent the singlet and doublet states, respectively. Legend: gray: carbon, blue: nitrogen, and cyan: hydrogen.

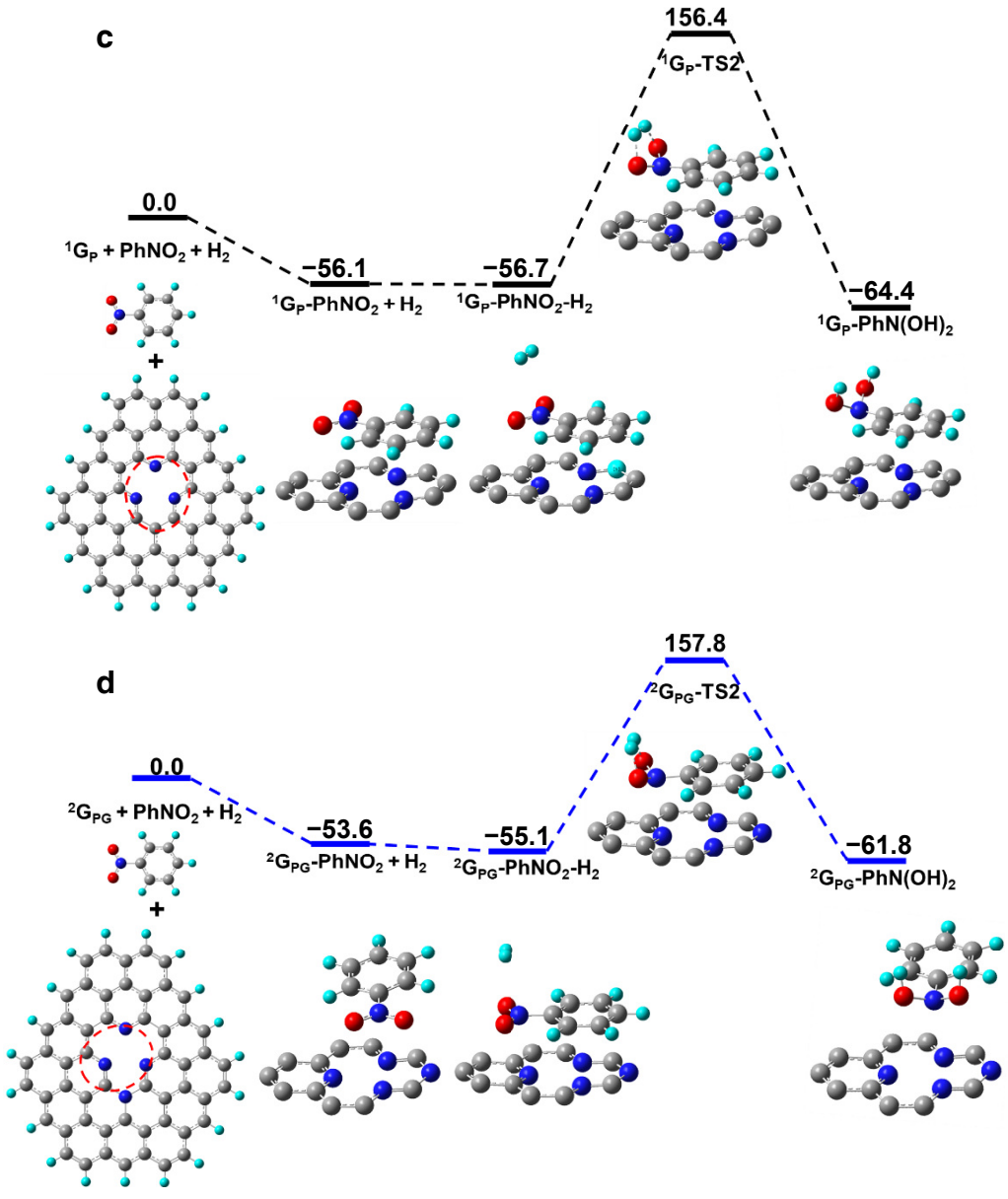


**Fig. 5.** Continued.

verifying that the reaction pathway following the stepwise adsorption of nitrobenzene and molecular hydrogen is feasible. It should be noticed that the apparent activation energy in protonic isopropanol is 53.8 kJ·mol$^{-1}$, much lower than that in non-protonic acetonitrile. This result re-emphasizes the importance of solvent and transfer hydrogenation in the metal-free hydrogenation, which may offer new opportunity to enhanced activity and new insight into the hydrogenation catalysis.

## 3 Conclusions

In summary, our study has demonstrated the efficacy of NCNTs as metal-free catalysts for the hydrogenation of nitrobenzene to aniline. An unexpected finding reveals that as the nitrogen content in NCNTs increases, the catalytic activity actually decreases. Meanwhile, NCNTs do not directly dissociate $H_2$ molecules, as evidenced by the absence of hydrogen radicals in EPR experiments. Those behaviors contrast sharply with metal-catalyzed hydrogenation reactions and highlight the unique catalytic mechanism employed by NCNTs. Furthermore, the transfer hydrogenation plays a significant role in boosting the overall reaction rate in protic solvents, suggesting the complex interplay between different reaction pathways in the metal-free catalytic hydrogenation. Combining kinetics experiments and DFT calculations, we propose that the hydrogenation of nitrobenzene catalyzed by NCNTs proceeds via an Eley–Rideal mechanism, where $H_2$ molecules are activated on the adsorbed nitrobenzene molecules, resulting in the zero-order and first-order kinetics with respect to nitrobenzene and $H_2$, respectively. The identification of $N_G$ and $N_P$ as the primary active sites in NCNTs offers important insights into the catalytic process. However, the synergistic interaction between $N_P$ and $N_G$ at higher nitrogen contents can be detrimental to the catalytic activity, suggesting that the optimization of nitrogen doping levels is crucial for achieving high performance. These insights offer theoretical guidance for the rational design of metal-free catalysts for catalytic hydrogenation reactions, paving the

way for the development of more sustainable and eco-friendly catalytic processes.

## 4 Experiments and methods

### 4.1 Materials

CNTs were provided by Zhongshan Canite Plastics Co., Ltd. Nitrobenzene, aniline, isopropanol, pyridine, toluene, and acetonitrile were purchased from Shanghai Aladdin biochemical Technology Co., Ltd. and used without further purification.

### 4.2 Catalyst preparation

For the elimination of residual synthesis catalysts, CNTs were agitated in concentrated HCl using a magnetic stirrer for 24 h. Subsequently, the mixture was diluted, filtered, and rinsed with deionized water until reaching a pH of 6–7. Finally, the CNTs were dried in ambient air at 100 °C overnight. NCNTs were synthesized through a chemical vapor deposition (CVD) process with pyridine, wherein CNTs were enveloped with a nitrogen-doped carbon layer and pyridine served as the nitrogen source for this synthesis method[35]. The pyridine deposition method for nitrogen-doped carbon materials offers notable advantages: It ensures uniform nitrogen deposition on the carbon surface for high doping efficiency, simplifies the process by dual-functioning as nitrogen and carbon source, and is straightforward and scalable for large-scale production. Briefly, 100 mg of purified CNTs were positioned on a quartz boat at the center of a horizontal quartz tube with an inner diameter of 4 cm. The quartz tube was then heated to a specific temperature in an argon atmosphere flowing at a rate of 200 mL·min$^{-1}$. Pyridine was subsequently injected using a syringe pump at a rate of 1.5 mL·h$^{-1}$ to initiate the deposition reaction. The resulting catalyst samples were labeled as NCNTs-*t*-*T*, where "*t*" represents the duration of the deposition reaction in hours, and "*T*" represents the pyrolysis temperature in degrees Celsius. Unless otherwise specified, the catalysts were prepared at 760 °C, abbreviated as NCNTs-*t*. To tune the nitrogen content, the mixture of pyridine and toluene was used as nitrogen source to prepare nitrogen-doped carbon material catalysts, named NCNT*xy*-0.5h, where *xy* represents the volumetric ratio of pyridine and toluene in *x*/*y*.

### 4.3 Characterizations of catalysts

The Brunauer–Emmett–Teller (BET) specific surface areas were determined through $N_2$ adsorption at 77 K in an ASAP 2010 analyzer. Raman spectra were acquired using a LabRAM Aramaic micro Raman spectrometer, employing an excitation wavelength of 514 nm with a 2 μm spot size. XPS analyses were conducted utilizing a Kratos Axis Ultra (DLD) spectrometer equipped with an Al K$\alpha$ X-ray source, with binding energies (±0.2 eV) referenced to the C 1s peak at 284.6 eV. EPR spectra were recorded using an X-band on a Bruker EMX spectrometer.

### 4.4 Selective hydrogenation reaction

The nitrobenzene hydrogenation reaction was conducted in a high-pressure reactor with a volume of 50 mL. The procedure was outlined as follows: 50 mg of catalyst, 18 mL of solvent, and 0.5 g of nitrobenzene were combined in a polytetrafluoroethylene-lined vessel, which were then transferred into the high-pressure reactor. Subsequently, hydrogen gas was used to purge the reactor three times to remove any air present. The stirring speed of the reactor was set at 1100 rpm while gradually heating up. Once the specified temperature was reached, $H_2$ was introduced, marking the beginning of the reaction time. After the reaction, the reactor was cooled down, and 0.3 g of toluene was added as an internal standard. The mixture was thoroughly stirred and then filtered using an organic filter membrane with a pore size of 0.22 μm to obtain the test filtrate. The catalyst was filtered and products were determined by gas chromatography-mass spectroscopy (GC-MS). The quantitative analysis of the reaction products was carried out by GC (Agilent 7890N) equipped with a FID detector and a DB-1701 capillary column.

### 4.5 DFT calculation

All geometric calculations in this study were conducted using the Gaussian 09 program package[36]. The self-consistent reaction field (SCRF) method, based on the universal solvation model SMD[37], was employed to assess the influence of $CH_3CN$ solvent. Dispersion corrections were computed during optimization using Grimme's D3(BJ) method[38]. The natural charges and dominant occupancies of natural bond orbitals (NBOs) were evaluated using the NBO analysis[39]. The frequency analyses for all structures were performed at B3LYP-D3(BJ)/6-31+G(d)(SMD, $CH_3CN$) level of theory to obtain all energies.

## References

[1] Wang, D.; Astruc, D. The golden age of transfer hydrogenation. *Chem. Rev.* **2015**, *115*, 6621–6686.
[2] Patel, M.; Savaram, K.; Li, Q. D.; Buchspies, J.; Ma, N.; Szostak, M.; He, H. X. Carbon-based, metal-free catalysts for chemical catalysis. In *Carbon-Based Metal-Free Catalysts: Design and Applications*. Dai, L. M., Ed.; Wiley-VCH: Weinheim, 2018; pp 597–657.
[3] Su, D. S.; Wen, G. D.; Wu, S. C.; Peng, F.; Schlögl, R. Carbocatalysis in liquid-phase reactions. *Angew. Chem., Int. Ed.* **2017**, *56*, 936–964.
[4] Kong, X. K.; Sun, Z. Y.; Chen, M.; Chen, C. L.; Chen, Q. W. Metal-free catalytic reduction of 4-nitrophenol to 4-aminophenol by N-doped graphene. *Energy Environ. Sci.* **2013**, *6*, 3260–3266.
[5] Wei, Q. H.; Qin, F. F.; Ma, Q. X.; Shen, W. Z. Coal tar- and residual oil-derived porous carbon as metal-free catalyst for nitroarene reduction to aminoarene. *Carbon* **2019**, *141*, 542–552.
[6] Chen, X. H.; Shen, Q. J.; Li, Z. J.; Wan, W. H.; Chen, J. Z.; Zhang, J. Y. Metal-free $H_2$ activation for highly selective hydrogenation of nitroaromatics using phosphorus-doped carbon nanotubes. *ACS Appl. Mater. Interfaces* **2020**, *12*, 654–666.
[7] Li, B. J.; Xu, Z. A nonmetal catalyst for molecular hydrogen activation with comparable catalytic hydrogenation capability to noble metal catalyst. *J. Am. Chem. Soc.* **2009**, *131*, 16380–16382.
[8] Welch, G. C.; San Juan, R. R.; Masuda, J. D.; Stephan, D. W. Reversible, metal-free hydrogen activation. *Science* **2006**, *314*, 1124–1126.
[9] Chen, D. J.; Wang, Y. T.; Klankermayer, J. Enantioselective hydrogenation with chiral frustrated lewis pairs. *Angew. Chem., Int. Ed.* **2010**, *49*, 9475–9478.
[10] Liu, Q.; Liao, Q. B.; Hu, J. L.; Xi, K.; Wu, Y. T.; Hu, X. B. Covalent organic frameworks anchored with frustrated Lewis pairs for hydrogenation of alkynes with $H_2$. *J. Mater. Chem. A* **2022**, *10*, 7333–7340.
[11] Primo, A.; Neatu, F.; Florea, M.; Parvulescu, V.; Garcia, H. Graphenes in the absence of metals as carbocatalysts for selective acetylene hydrogenation and alkene hydrogenation. *Nat. Commun.* **2014**, *5*, 5291.
[12] Zhang, Y.; Lan, P. C.; Martin, K.; Ma, S. Q. Porous frustrated Lewis pair catalysts: Advances and perspective. *Chem Catal.* **2022**, *2*, 439–457.
[13] Ding, Y. X.; Huang, X.; Yi, X. F.; Qiao, Y. X.; Sun, X. Y.; Zheng, A. M.; Su, D. S. A heterogeneous metal-free catalyst for hydrogenation: Lewis acid-base pairs integrated into a carbon lattice. *Angew. Chem., Int. Ed.* **2018**, *57*, 13800–13804.
[14] Shan, J. X.; Sun, X. Q.; Zheng, S. Y.; Wang, T. D.; Zhang, X. W.; Li, G. Z. Graphitic N-dominated nitrogen-doped carbon nanotubes as

efficient metal-free catalysts for hydrogenation of nitroarenes. *Carbon* **2019**, *146*, 60–69.
[15] Chi, Y. Q.; Zheng, S. Y.; Zhang, X. W.; Li, G. Z. Chitosan derived N-doped carbon nanotubes for selective hydrogenation of nitroarenes to anilines. *Int. J. Hydrogen Energy* **2021**, *46*, 36124–36136.
[16] Xiong, W.; Wang, Z. N.; He, S. L.; Hao, F.; Yang, Y. Z.; Lv, Y.; Zhang, W. B.; Liu, P. L.; Luo, H. A. Nitrogen-doped carbon nanotubes as a highly active metal-free catalyst for nitrobenzene hydrogenation. *Appl. Catal. B: Environ.* **2020**, *260*, 118105.
[17] Luo, Z. C.; Nie, R. F.; Nguyen, V. T.; Biswas, A.; Behera, R. K.; Wu, X.; Kobayashi, T.; Sadow, A.; Wang, B.; Huang, W. Y. et al. Transition metal-like carbocatalyst. *Nat. Commun.* **2020**, *11*, 4091.
[18] Chase, P. A.; Welch, G. C.; Jurca, T.; Stephan, D. W. Metal-free catalytic hydrogenation. *Angew. Chem., Int. Ed.* **2007**, *46*, 8050–8053.
[19] Zhou, Z.; Gao, X. P.; Yan, J.; Song, D. Y. Doping effects of B and N on hydrogen adsorption in single-walled carbon nanotubes through density functional calculations. *Carbon* **2006**, *44*, 939–947.
[20] Ulbricht, H.; Moos, G.; Hertel, T. Interaction of molecular oxygen with single-wall carbon nanotube bundles and graphite. *Surf. Sci.* **2003**, *532–535*, 852–856.
[21] Han, D.; Liu, Y.; Lv, Y.; Xiong, W.; Hao, F.; Luo, H. A.; Liu, P. L. *In situ* oxygen-induced zigzag graphene as metal-free catalyst for hydrogen activation in nitroarenes hydrogenation. *Carbon* **2023**, *203*, 347–356.
[22] Fu, H. Q.; Huang, K. T.; Yang, G. X.; Cao, Y. H.; Wang, H. J.; Peng, F.; Wang, Q.; Yu, H. Synergistic effect of nitrogen dopants on carbon nanotubes on the catalytic selective epoxidation of styrene. *ACS Catal.* **2020**, *10*, 129–137.
[23] Wang, X.; Zhao, H.; Zhou, Y.; Yin, C.; He, W.; Feng, F.; Wang, F.; Lu, C.; Li, X. Yeast-derived N, P co-doped porous green carbon materials as metal-free catalysts for selective hydrogenation of chloronitrobenzene. *Green Chemistry* **2024**, *26*, 7958–7970.
[24] Deng, Y. C.; Gao, R.; Lin, L. L.; Liu, T.; Wen, X. D.; Wang, S.; Ma, D. Solvent tunes the selectivity of hydrogenation reaction over α-MoC catalyst. *J. Am. Chem. Soc.* **2018**, *140*, 14481–14489.
[25] Michel, C.; Gallezot, P. Why is ruthenium an efficient catalyst for the aqueous-phase hydrogenation of biosourced carbonyl compounds. *ACS Catal.* **2015**, *5*, 4130–4132.
[26] Carley, A. F.; Edwards, H. A.; Mile, B.; Roberts, M. W.; Rowlands, C. C.; Jackson, S. D.; Hancock, F. E. An EPR study of a palladium catalyst using a PBN (N-benzylidene-tert-butylamine N-oxide) spin trap: Direct demonstration of hydrogen spillover. *J. Chem. Soc. Chem. Commun.* **1994**, 1407–1408.
[27] Burt, A.; Emery, M.; Maher, J.; Mile, B. Electron spin resonance allied with spin traps to detect and identify atoms and radicals on Pd-supported catalyst surfaces in solution. *Magn. Reson. Chem.* **2001**, *39*, 85–88.
[28] Wang, H.; Shi, Y. Z.; Wang, Z. W.; Song, Y. J.; Shen, M. C.; Guo, B. B.; Wu, L. Selective hydrogenation of cinnamaldehyde to hydrocinnamaldehyde over Au-Pd/ultrathin $SnNb_2O_6$ nanosheets under visible light. *J. Catal.* **2021**, *396*, 374–386.
[29] Al-Madanat, O.; Nunes, B. N.; AlSalka, Y.; Hakki, A.; Curti, M.; Patrocinio, A. O. T.; Bahnemann, D. W. Application of EPR spectroscopy in $TiO_2$ and $Nb_2O_5$ photocatalysis. *Catalysts* **2021**, *11*, 1514.
[30] Wang, X. D.; Cárdenas-Lizana, F.; Keane, M. A. Toward sustainable chemoselective nitroarene hydrogenation using supported gold as catalyst. *ACS Sustain. Chem. Eng.* **2014**, *2*, 2781–2789.
[31] Cai, S. F.; Duan, H. H.; Rong, H. P.; Wang, D. S.; Li, L. S.; He, W.; Li, Y. D. Highly active and selective catalysis of bimetallic $Rh_3Ni_1$ nanoparticles in the hydrogenation of nitroarenes. *ACS Catal.* **2013**, *3*, 608–612.
[32] Corma, A.; Concepción, P.; Serna, P. A different reaction pathway for the reduction of aromatic nitro compounds on gold catalysts. *Angew. Chem., Int. Ed.* **2007**, *46*, 7266–7269.
[33] Wang, H. H.; Zhang, W.; Liu, Y. Q.; Pu, M.; Lei, M. First-principles study on the mechanism of nitrobenzene reduction to aniline catalyzed by a N-doped carbon-supported cobalt single-atom catalyst. *J. Phys. Chem. C* **2021**, *125*, 19171–19182.
[34] Hu, X. W.; Long, Y.; Fan, M. Y.; Yuan, M.; Zhao, H.; Ma, J. T.; Dong, Z. P. Two-dimensional covalent organic frameworks as self-template derived nitrogen-doped carbon nanosheets for eco-friendly metal-free catalysis. *Appl. Catal. B: Environ.* **2019**, *244*, 25–35.
[35] Tian, G. L.; Zhang, Q.; Zhang, B. S.; Jin, Y. G.; Huang, J. Q.; Su, D. S.; Wei, F. Toward full exposure of "active sites": Nanocarbon electrocatalyst with surface enriched nitrogen for superior oxygen reduction and evolution reactivity. *Adv. Funct. Mater.* **2014**, *24*, 5956–5961.
[36] Frisch, M. J.; Trucks, G. W.; Schlegel, H. B.; Scuseria, G. E.; Robb, M. A.; Cheeseman, J. R.; Scalmani, G.; Barone, V.; Mennucci, B.; Petersson, G. A. et al. *Gaussian 09, Revision d. 01*; Gaussian. Inc.: Wallingford, 2009.
[37] Marenich, A. V.; Cramer, C. J.; Truhlar, D. G. Universal solvation model based on solute electron density and on a continuum model of the solvent defined by the bulk dielectric constant and atomic surface tensions. *J. Phys. Chem. B* **2009**, *113*, 6378–6396.
[38] Grimme, S.; Antony, J.; Ehrlich, S.; Krieg, H. A consistent and accurate *ab initio* parametrization of density functional dispersion correction (DFT-D) for the 94 elements H-Pu. *J. Chem. Phys.* **2010**, *132*, 154104.
[39] Reed, A. E.; Curtiss, L. A.; Weinhold, F. Intermolecular interactions from a natural bond orbital, donor–acceptor viewpoint. *Chem. Rev.* **1988**, *88*, 899–926.

## Data availability

All data needed to support the conclusions in the paper are presented in the manuscript and the Supplementary Information. Additional data related to this paper may be requested from the corresponding author upon request.

## Acknowledgements

This work was sponsored by the National Natural Science Foundation of China (No. 22272056), Natural Science Foundation of Sichuan, China (No. 2023NSFSC0966), Natural Science Foundation of Guangdong Province (Nos. 2024B1515040016 and 2023A1515012804), and Science and Technology Program of Guangzhou (No. 2023A04J0674). The work of DFT calculation was carried out at Information and Network Engineering and Research Center in South China University of Technology, and the calculations were performed on SCUTGrid.

## Author contributions

H. Q. F., J. L. Z., and H. Y. designed the experiments. H. Y. supervised the project. H. Q. F., and K. T. H. performed the experiments and carried out characterizations. All authors discussed the experiments and results. H. Q. F., and H. Y. prepared and revised the manuscript.

## Competing interests

The authors have no competing interests to declare that are relevant to this article.

## Use of AI statement

None.

## Additional information

**Supplementary Information** The online version contains supplementary material available at https://doi.org/10.26599/CF.2025.9200028.